Immune Remodelling of the Extracellular Matrix Drives Loss of Cancer Stem Cells and Tumor Rejection

Ana Pires[1]*, Alexander Greenshields-Watson[1]*, Emma Jones[1]*, Kathryn Smart[1], Sarah N Lauder[1], Michelle Somerville[1], Stefan Milutinovic[1], Howard Kendrick[2], James P. Hindley[3], Rhiannon French[2], Matthew J. Smalley[2], William J. Watkins[1], Robert Andrews[4], Andrew Godkin[1^] and Awen Gallimore[1^].

* and ^ Equal Contribution

[1] Infection and Immunity, School of Medicine, Cardiff University, Henry Wellcome Building, University Hospital of Wales, Cardiff, UK.

[2] European Cancer Stem Cell Research Institute, Cardiff University, Hadyn Ellis Building, Cardiff, UK.

[3] Indoor Biotechnologies, Vision Court, Cardiff, UK.

[4] Systems Immunity Research Institute, Cardiff University, Cardiff, UK.

Running title: Effective Immunity Drives Tumor Remodelling and Loss of CSCs

Keywords: Immunotherapy, Microenvironment, Extracellular Matrix, Lymphatics, Cancer Stem Cells

Financial support: This work was supported by a program grant from Cancer Research UK (C16731/A21200), Cancer Research Wales (5272BR) an MRC-funded studentship (AP), a Breast Cancer Now project grant (PR1377) and a Wellcome Trust collaborator award (grant 209213/Z/17/Z).

Corresponding author: Ana Pires
Henry Wellcome Building, School of Medicine, Heath Park, Cardiff CF14 4XN
+44 (0)29 2068 7081
PiresAC@cardiff.ac.uk

Declaration of interests
The authors declare no conflict of interest.

Word count: 4,269 words
Number of Figures: 6 Figures (+ 8 Supplementary Figures)

Abstract

The nature of the tumor microenvironment (TME) influences the ability of tumor-specific T cells to control tumor growth. In this study we performed an unbiased comparison of the TME of Treg-replete and Treg-depleted carcinogen-induced tumors, including Treg-depleted responding (regressing) and non-responding (growing) tumors. This analysis revealed an inverse relationship between extracellular matrix (ECM) and T cell infiltrates where responding tumors were T cell rich and ECM poor whereas the converse was observed in non-responder tumors. For this reason, we hypothesised that the ECM acted as a barrier to successful T cell infiltration and tumor rejection. However, further experiments revealed that this was not the case but instead showed that an effective T cell response dramatically altered the density of ECM in the TME. Along with loss of ECM and high numbers of infiltrating T cells, responder tumors were distinguished by the development of lymphatic and blood vessel networks with specialized immune function. ECM-rich tumors exhibited a stem cell-like gene expression profile and superior tumor-initiating capacity, whereas such features were absent in responder tumors. Overall, these findings define an extended role for an effective immune response, not just in direct killing of tumor cells, but in widescale remodelling of the TME to favor loss of ECM, elimination of cancer stem cells, and propagation of adaptive immunity.

Introduction

Variable responses to cancer immunotherapies are well documented amongst and within different cancer types (1,2). While the extent of T cell activation is crucial for treatment success, there is evidence that other features of the tumor microenvironment (TME) act as barriers or enablers of immune attack. The type of stromal cells present, the nature of blood vessels, the composition of the extracellular matrix (ECM), and tumor intrinsic gene expression pathways may all influence tumor growth directly as well as affect the ability of T cells to infiltrate and/or function effectively (3-8). Conversely, other anatomical features are associated with productive immune responses, namely the presence of specialised vasculature termed high endothelial venules (HEV), which can be induced by immunotherapy and are often associated with development of tertiary lymphoid structures (9).

It remains unclear the extent to which the pre-existing TME prevents development of an effective immune response or whether an effective immune response alters the TME. In support of the latter, using a mouse model of

carcinogen-induced fibrosarcomas (3,4), we found that targeting Foxp3^{+} regulatory T cells (Tregs) results in significant control of tumor growth in approximately half of tumor-bearing mice. These mice, termed “responders” could be distinguished from “non-responder” mice by presence of intratumoral HEV and a significantly higher number of tumor-infiltrating T cells (TILs) (3,4). HEV were not identified in untreated mice, implying that development of HEV was a consequence of successful immunotherapy. Other studies using adoptively transferred T cells or PD-1 blockade have similarly shown that activated T cells can alter tumor blood vessels in a manner that promotes tumor immunity (5,10).

To explore the concept that T cells modulate the TME beyond tumor blood vessels, we have used a variety of tools to identify features distinguishing the TME of responding and non-responding tumors and their relationship to the TME of untreated tumors. Specifically, we questioned whether the TME dictated responses to immunotherapy or whether the nature of the response to immunotherapy overcame the suppressive conditions of the TME. Overall, our data indicated that a successful response to immunotherapy drove events which ultimately promoted tumor regression through removal of cancer stem cells (CSC), TME remodelling and amplification of the adaptive immune response.

Material and Methods

Mice, Induction of Tumors and Depletion of Tregs

B6.129(Cg)-*Foxp3*$^{tm3(DTR/GFP)Ayr}$/J mice used in this study were gratefully given to us by Professor Alexander Rudensky (11). Female Balb/c mice were purchased from Charles River. Mice were housed in accordance with UK Home Office regulations, and isolator-bred before being housed in filter-top cages for the experiments. Fibrosarcomas were induced in 8-15 week old Foxp3^{DTR} mice by subcutaneous injection with 400 μg of 3-methylcholanthrene carcinogen (MCA) suspended in 100 μL of olive oil into the left hind leg (12). Mice were monitored for up to 18 weeks. Tumor-bearing mice were sacrificed before tumors reached 1.5 cm in diameter (measured with calipers), or if tumors caused discomfort. Upon dissection, tumors were resected avoiding local muscle, other normal tissues and the local popliteal lymph node. Tumor measurements and growth rate calculations were

performed as previously described (4). To ensure complete depletion of Tregs, doses of diphtheria toxin (DT) were selected based on dose-optimisation performed in a previous study (3). DT, diluted in sterile PBS was administered by intra-peritoneal injection at a dose of 15 μg/kg body weight every other day, after development of a palpable tumor. Tumors were variable sizes at the start of treatment, hence growth rates and not absolute tumor sizes were compared in order to evaluate treatment-response.

The tumor cell line 4T1, obtained from ATCC in 2014 (CRL-2539, not authenticated in the past year), was cultured for 10-14 days before being injected subcutaneously into the mammary fat pad of Balb/c mice. These cells were regularly tested and found to be negative for mycoplasma infection. 10^5 were injected subcutaneously into the mammary fat pad of Balb/c mice. PI-3065, a small molecule inhibitor of the PI3K delta subunit provided by Genentech, was administered by oral gavage at a dose of 75 mg/kg, vehicle treated mice were given an equivalent volume of carrier solution. Mice were dosed daily from day -1 prior to tumor inoculation until experiment termination. Animal studies were conducted with approval of the UK Home Office.

Immunofluorescence Staining and Microscopy

5 μm sections of frozen tissue embedded in OCT (KMA-0100-00A, CellPath) were fixed in ice-cold acetone, and non-specific binding blocked with 2.5% normal horse serum (S-2012-50, VectorLabs). Sections were incubated in primary antibody overnight at 4°C, washed with PBS, incubated in secondary antibody, washed again, counterstained with Hoechst (14533, Sigma) and then mounted in ProLong Gold Antifade mountant (P36930, ThermoFisher Scientific). Primary antibodies were used as follows: anti-TNC (ab108930, abcam) 1 μg/mL, anti-CD3 (GA50361-2, Agilent) 2 μg/mL, anti-GZMB (AF1865, R&D Systems) 0.4 μg/mL, anti-CD8 (42-0081-82, ThermoFisher) 1 mg/mL, anti-Lumican (AF2745, R&D Systems) 0.4 μg/mL, anti-LYVE-1 (14-0443-82, ThermoFisher), anti-CCL21 (AF457, R&D Systems) 5 μg/mL, anti-ZEB1 (HPAO27524, Atlas Antibodies) 0.2 μg/mL, anti-CD206 (AF2535, R&D Systems) 0.3 mg/mL, and anti-MHC class II (NBP1-43312, Novus Biologicals) 20 μg/mL. Sections were imaged using a Zeiss Axioscan.Z1 Slide Scanner and analysed using Zen software Blue edition. Immune cells were counted per high power field of view, and an average of 10 fields of view was calculated per section.

TNC quantification

Images were analysed for TNC using QuPath software version 0.2.0 milestone 11 (13), quantified using the pixel classifier tool, and results shown in percentage of positive TNC pixels per mm^2 of tissue.

RNAscope

TNC mRNA in situ hybridization was measured with RNAscope assay, developed by Advanced Cell Diagnostics (ACD) according to the manufacturer's protocols. Briefly, tumor sections were deparaffinized, incubated with hydrogen peroxide at room temperature for 10 min, boiled with target retrieval solution for 15 min, and then treated with protease plus at 40°C for 30 min. Sections were hybridized with Mm-Tnc probe (465021, ACD), Mm-Ppib probe as positive control (313911, ACD) and DapB probe as negative control (310043, ACD) at 40°C for 2 h. Hybridization signals were amplified with RNAscope 2.0 HD reagent kit-red (322350, ACD). Sections were imaged using a Zeiss Axioscan.Z1 Slide Scanner and higher power images were captured using a Zeiss Apotome Axio Observer.

Cell line establishment

To establish cell lines derived from MCA-induced tumours, two untreated tumours were dissected, chopped into small pieces and incubated in a cell culture flask with R10 media (RPMI media (Gibco) supplemented with 10% Foetal Calf Serum (FCS, Gibco), L-glutamine and penicillin/streptomycin) at 37°C and 5% CO_2. The following day, pieces of tissue were removed, and media was replaced, to exclude cells that did not attach to the flask. Cells were split up to 3 times a week and, once these were expanded, cells were frozen at -80°C, in single vials of 10^7 cells/mL of freezing media (FCS with 10% DMSO (Sigma)). Cell lines (MCA-GG1 and MCA-GG2) were grown from each tumour and were left to grow for 3-6 passages before being injected into mice.

Lentivirus production and tumor cell injection

Oligonucleotide pairs for sh*TNC* (CACCGCCCTTGGCTGAAATTGATAGCGAACTATCAATTTCAGCCAAGGGC and AAAAGCCCTTGGCTGAAATTGATAGTTCGCTATCAATTTCAGCCAAGGGC) were ligated into pENTR/U6 Gateway system entry vector (K4944-00 and K4945-00,

Invitrogen) according to the manufacturer's instructions. A scrambled plasmid was generated as control. Hairpin sequences were verified by transduction of the virus on test cells and knock down levels measured by qPCR. Sequences were then transferred and viral supernatants were generated as described (14). MCA-GG2 cells were resuspended at 10^6 cells/mL in viral supernatant and plated at 1 mL/well in ultra-low attachment 24-well plates. After 16 hours, cells were washed and replated in RPMI 1640 medium (Gibco, Fisher Scientific) supplemented with 10% foetal bovine serum (Gibco, Fisher Scientific), and L-glutamine and penicillin/streptomycin. After 48 hours, cells were transferred to normal tissue culture plastic and maintained in growth medium for one week. After this time, cells were trypsinized and flow sorted to isolate GFP^+ cells for qPCR analysis. Mice aged 8-15 weeks were anesthetized and injected subcutaneously with $0.5x10^6$ control or knockdown cells into the left hind leg. Mice were monitored, and tumors were measured as described above.

Quantitative real-time PCR

A sample of each cell line was collected, and cells were disrupted with 500 μL of RLT buffer. RNA was purified with RNeasy Mini Kits (74104, Qiagen), according to the manufacturer's instructions, and quantified using a NanoDrop 2000 spectophotometer (ThermoFisher Scientific). DNase treatment and cDNA synthesis were performed using High-Capacity RNA-to-cDNA Kit (4387406, Applied Biosystems), according to the manufacturer's instructions. Quantitative real-time PCR reaction was performed in a final volume of 20 μL, containing 2 μL of cDNA sample, 10 μL of Gene Expression TaqMan Master Mix (4369514, Applied Biosystems) and 1 μL of TaqMan Gene Expression Assay probes. Probes used were mouse beta-actin (4352341E, Applied Biosystems), as housekeeping gene, and *Tnc* (Mm00495662_m1, Applied Biosystems) as target gene. Reactions were performed in triplicate on an Applied Biosystems QuantStudio 3 Real Time Machine. Relative expression of mRNA was calculated using the ΔΔCt method.

Bioinformatic analyses – Mouse Data

Microarray data was previously published (4). Probe intensity values were corrected by background subtraction using Genome Studio software and subsequently log-2 and baseline (median) transformed using Genespring software (Agilent). Differential expression analysis was performed using the R package 'Limma' (15), only probes with the highest baseline average were used in heatmaps

and later analyses. The 'parallelDist' R package was used to perform Manhattan distance analysis of all genes. Heatmaps were created using the pheatmap R package (hierarchical clustering method: ward.D2 using Manhattan distance). All pathway analysis was carried out using the 'ReactomePA' R package (16) or gene sets downloaded from the Reactome database with conversion of gene IDs to mouse nomenclature using the 'biomaRt' R package (17). Code available at https://github.com/ALGW71/ImmuneRemodellingECM. Raw microarray data is available at ArrayExpress accession E-MTAB-9351.

CIBERSORT (18) analysis was performed on the pre normalised microarray data using the immune deconvolution package in R (https://github.com/icbi-lab/immunedeconv) (19). The CIBERSORT binary for use in R was obtained from the website: https://cibersort.stanford.edu/ following registration and approval of access (16th April 2020).

Bioinformatic analyses – Human data

Level 3 (raw counts, htseq.counts.gz) RNAseq data, and sample meta data (GDC sample sheet and clinical cart files) were download from The Cancer Genome Atlas (TCGA) GDC portal (https://portal.gdc.cancer.gov/) on 3-October-2019 for 21 cancer types. All datasets were normalised as one matrix within the 'DESeq2' Bioconductor package (20) in R and the DESeq2 normalised counts were used for all analyses.

Only data from primary tumors was used for analysis. Patient information (GDC sample sheet - vital status, days to death, days to last follow up) was used for Kaplan Meier survival analysis (R packages: 'survminer' and 'survival'). Data was censored at days-to-last-follow-up or days-to-death and log-rank p values calculated between two curves. Medoids clustering was performed using the 'ClusterR' package. Clustering was carried out on expression data, centre and scaled by each gene, using the Manhattan distance metric to obtain two clusters. RNAseq data from distinct cancers was not combined to perform clustering, this ensured gene expression levels from different cancer types were not unfairly compared.

To cluster on cytotoxic T lymphocytes (CTLs) alone, a meta gene signature from (21) was used (CTL genes – *CD3G*, *CD3E*, *CD3D*, *PTPRC*, *CD8A*; cytotoxicity genes – *PRF1*, *GZMH*, *GNLY*, *GZMB*, *GZMK*, *GZMA*) in each cancer type. Sixteen cancers in which CTL signature was prognostic of survival, based on visual inspection of survival curves, were taken forward for TNC clustering. CTL-high and

CTL-low clusters were separated, and a second round of medoids clustering was performed on based expression of TNC resulting in four groups. Several R packages from the 'Tidyverse' were used to data wrangling and visualisation (22). Code is available at https://github.com/ALGW71/ImmuneRemodellingECM.

Tumorsphere formation assay

Live single cells obtained from untreated, non-responder and responding tumors were seeded at 10^4 cells/mL in 96-well ultra-low attachment plates (3474, Corning) and cultured in DMEM/F12 (ThermoFisher Scientific) with N2 (17502048, ThermoFisher Scientific), 10ng/mL EGF (PMG8043, ThermoFisher Scientific), and 10ng/mL FGF (PMG0033, ThermoFisher Scientific). After 7 days, spheres were counted under an inverted phase microscope (Nikon), and passaged. After 14 days, spheres were counted again, under the same conditions.

Statistical analyses

The statistical difference between pairs of groups was assessed dependent on the normality of the data, through either nonparametric Kruskal-Wallis with Dunn's multiple comparison test or one-way ANOVA with Tukey post-test. A P value < 0.05 was considered significant. Statistical analyses were performed using GraphPad Prism software, version 8.4.3.

Results

Expression patterns of T cells and TNC in responders or non-responder tumors

Using Foxp3^{DTR} mouse model to deplete Tregs in the presence of carcinogen-induced fibrosarcomas, we report that the antitumor response following Treg depletion is variable (3,4). The mouse group defined as "non-responders" have tumors without HEVs and have no significant decrease in tumor growth rates or increase in TILs after Treg depletion compared to untreated mice. Conversely, "responders" have HEVs in their tumors and overall show a significant decrease in tumor growth rate and a significant increase in TILs after Treg depletion (summarised

in Fig. 1A and ref 3 and 4). In this model, both neogenesis of HEV and control of tumor growth is strictly T cell-dependent (4). In these previous studies, the extent of Treg depletion is comparable in all treated mice, ruling out a differential effect of the DT in individual animals (3).

To further examine differences between the tumor types, we compared the transcriptomes of untreated, responder and non-responder tumors. In this analysis, we failed to find any genes that were differentially expressed (statistical test, padj less than 0.05) between non-responder and untreated tumors (Fig. 1B) whilst 20 genes were significantly higher in non-responder *versus* responder tumors (Fig. 1C), of which, the gene encoding the ECM protein, tenascin-C (*Tnc*) was most differentially expressed (padj = 0.025, logFC = 2.365). TNC, a protein known to have important roles in embryonic development and wound healing, is thought to impede T cell function and is often associated with poor cancer prognosis, local recurrence and metastasis (23-26).

When the transcriptomes of responder and non-responder tumors were compared, 74 genes emerged as having significantly higher expression in responder *versus* non-responder tumors (Fig. 1D). These revealed a significant enrichment of immune pathways (Supplemental Fig. S1A). *Cd6* (padj = 0.019, logFC = -2.189), a T cell adhesion gene, and *Zap70* (0.019, -1.85), *Cd3d* (0.019, -2.38), *Cd3g* (0.030, -2.28) and *Cd3e* (0.020, -2.20), key mediators of TCR signalling, were among the most significant differentially expressed genes (Fig. 1D). Although there was a clear T cell immune signature present in the differentially expressed genes of responder mice (Supplemental Fig. S1A), no pathways were significantly enriched in the non-responder gene list in which *Tnc* was most highly expressed. Analysis of gene expression patterns relative to *Tnc* using a Manhattan distance metric (Supplemental Fig. S2) indicated that *Tnc* and *Zap70* consistently had opposing expression patterns across all samples with the largest Manhattan distance value (21.08).

TNC protein expression was next confirmed by immunofluorescence staining. We found that TNC was more abundant at tumor periphery, presenting a well-organised fibrillar pattern compared to the tumor centre (Supplemental Fig. S3A). TNC was abundant in non-responder tumors compared to responders and variable in untreated tumors (Fig. 1E and Supplemental Fig. S3B). RNAscope revealed that *Tnc* transcripts were clearly more abundant in untreated and non-responder tumors compared to responders (Fig. 1F) and were observed in tumor cells (Fig. 1G). The inverse relationship between TNC and the level of T cell infiltrate was striking (Fig.

1E) since responding tumors had high numbers of TILs, indicating that successful antitumor immunity was strongly associated with absence of TNC.

TNC Expression associated with a CTL signature Impacted Patient Survival

T cell infiltration of tumors (particularly CTLs) (27) and presence of TNC (25,28) demonstrate opposing correlations with survival in human cancers. However, aside from the data presented above, evidence of an antagonistic relationship between T cells and TNC has solely been demonstrated *in vitro* (28). We investigated the relationship between CTL gene signatures and *Tnc* expression in the context of survival, specifically searching for trends analogous to those revealed by the mouse data. For this purpose, we examined RNAseq datasets from primary tumors in TCGA, to determine whether there was a link between a favourable CTL gene signature and TNC expression.

We identified 14 cancers where survival was improved with a CTL gene signature (21) in patients' primary tumors (6 statistically significant, Supplemental Fig. S4A). This was performed using an unbiased medoids clustering approach where we first clustered the datasets based on expression of CTL genes (Supplemental Fig. S4A), followed by expression of *TNC* within each individual cancer (Supplemental Fig. S4B,C). This approach ensured that we were comparing expression of CTL genes or *TNC* within and not across different cancer types (see methods). We used this analysis to generate groups of CTL-high and CTL-low tumors (Fig. 2A) which were then separately clustered by *TNC* expression (Fig. 2B,C), revealing that although *TNC* expression had no impact on survival within CTL-low tumors ($P = 0.48$, Fig. 2C), low *TNC* expression was associated with a highly significant increase in survival within CTL-high tumors ($P = 0.00062$, Fig. 2B). When we reversed the analysis, clustering *TNC* high/low first, followed by CTL high/low, the same effect was apparent (Supplemental Fig. S5). These data were similar to those obtained in the mouse model above as they clearly indicated that a successful T cell response was associated with low *TNC* expression. The key question for the study described herein was whether TNC impinged on CTL activity in patients and mice resulting in poorer survival/outcome, or whether an effective immune response resulted in loss of TNC.

TNC Did Not impinge on Responsiveness to Treg Depletion

Previous reports have suggested that TNC can affect T cell function through multiple mechanisms (24,29-32) . With these in mind and our own mouse data indicating an association between control of tumor growth and loss of TNC (Fig. 1) corroborated by an analysis of TCGA data for multiple cancers (Fig. 2), we hypothesised that TNC prevented T cells from successfully controlling cancer. In the case of the fibrosarcoma mouse model described here, we postulated that high TNC expression impeded development of a successful T cell response generated after Treg depletion.

We first examined the relationship between TNC and the intratumoral distribution of T cells by identifying and enumerating T cells within high power images of tumor areas with high and low intensity of TNC staining (Supplemental Fig. S6). These comparisons were only possible in untreated and non-responder tumors, due to lack of TNC in responder tumors. Findings indicated that T cells were found in both areas and were even slightly more frequent in TNC high areas (Fig. 3A,B). Granzyme-B (GZMB) expression revealed significantly more $GZMB^{+}CD8^{+}$ T cells in TNC-high compared to TNC-low areas of non-responder tumors, suggesting that high expression of TNC might be associated with less degranulation of T cells in poorly controlled tumors (Fig. 3C,D).

Given the well documented role of macrophages in remodelling the TME, we analysed our microarray data using CIBERSORT to ascertain whether differences in the M0/M1/M2 phenotypes in responders and non-responders are apparent. This showed a strong M0 signature in untreated mice, but no significant differences between M1/M2 phenotypes between responders and non-responders, with a large variation between individual animals (Supplemental Fig. S8A). Tumor sections from non-responder and responder tumors were co-stained for TNC and CD206 or MHC class II. In agreement with the CIBERSORT findings, these data indicated no significant difference when comparing $CD206^{+}$ and $MHC\text{-}II^{+}$ cells between the different groups, or between TNC high and low areas (Supplemental Fig. S8B,C). Thus, we concluded that the loss of TNC was mainly associated with a robust T cell response.

To definitively address whether TNC impinges on a successful T cell response, we generated fibrosarcoma cell-lines from the MCA-induced tumors by *in vitro* culture of dissociated cells. These cell-lines were genetically modified using TNC-targeted shRNA (shTNC 3559) or control scrambled shRNA (shScr) and then injected into $Foxp3^{DTR}$ mice (Fig. 4A). Tumor growth was monitored, and Tregs

depleted once tumors were palpable. Although Treg depletion resulted in a reduction in tumor growth rate in both shScr and shTNC tumors (Fig. 4B and Supplemental Fig. S7), TNC expression did not affect tumor growth rate in either Treg-depleted or untreated tumors (Fig. 4B). It was striking that similar to the carcinogen-induced tumors, loss of TNC expression was observed in tumors responding to Treg-depletion (Fig. 4C). These findings indicate that although TNC may have impeded T cell responses, this effect could be overcome after Treg depletion. Moreover, the data pointed to loss of TNC expression being a consequence of an effective immune response.

We used a second, distinct mouse model of Treg-targeted immunotherapy to address whether TNC expression similarly alters as a response to successful immunotherapy. For this purpose, we used a model of triple negative breast cancer, namely the 4T1 cell-line which recapitulates features of aggressive breast cancer in Balb/c mice. Mice were inoculated with 4T1 cells and treated with PI-3065 previously shown to inactivate Tregs and promote control of tumor growth in treated mice (33). We selected untreated tumors, responder and non-responder treated tumors to compare TNC expression. A similar distribution was observed to the fibrosarcoma model whereby control of tumor growth was associated with a loss of TNC (Fig. 4D).

Alterations in TNC were Indicative of ECM Changes in Responder Tumors

The data described above indicated that although TNC did not inhibit development of a successful T cell response, loss of TNC was a consequence of a successful T cell response. We next wished to determine whether loss of TNC was indicative of other TME alterations. We first looked at genes with a less stringent padj < 0.10. When pathway analysis was applied to this list of 123 genes, the pathway “Extracellular Matrix Organisation” was the only significantly enriched pathway (Supplemental Fig. S1B, 12 genes, padj = 2.285e-05). An opposing pattern of expression of genes encoding these proteins was observed in non-responder versus responder tumors (Fig. 5A).

These data indicated that although focusing on TNC enabled us to evaluate the relationship between ECM, T cells and tumor growth, it was clear that TNC was not the only ECM protein over-represented in non-responder *versus* responder tumors. To examine this further, untreated, non-responder and responder tumors were stained with Lumican- and Collagen-specific antibodies (Fig. 5B,C); the staining

pattern was as observed for TNC thereby pointing to widescale alterations in the ECM composition in responder *versus* non-responder tumors.

Previous studies indicate that ECM-rich tumors are served by poor lymphatic networks, due to compression of the lymphatic vessels (33). To determine whether this was true for the tumors here, sections from untreated, non-responder and responder tumors were stained with LYVE-1- and CCL21-specific antibodies. The difference in the appearance of lymphatic vessels was striking (Fig. 5D). Robust staining was observed only in responder tumors, where lymphatics were characterised by the presence of CCL21 around LYVE-1 positive vessels entirely compatible with improved lymphatic function and potentially with an enhanced ability to guide dendritic cells (DCs) to lymphatic vessels (34). Overall, these findings point to widescale alterations to the TME characterised by a widescale loss of ECM and a reciprocal gain in immune function.

Cancer Cell Gene alterations in Responder versus Non-Responder Tumors

As part of the bioinformatic analysis, we mapped the expression pattern of *Tnc* against all other genes and samples in the microarray analysis using a Manhattan distance metric. In this way we could rank genes according to how similar or opposing/inverse their expression pattern was against *Tnc*. As already mentioned, this revealed that *Zap70* had the furthest distance (opposing expression pattern) from *Tnc*. In contrast, those with a similar pattern to *Tnc* included several cancer-associated (*Vegfa*, *Trib3*, *Uck2*) and stem cell/EMT genes (*Ttc3*, and *Twist2*). Given that dense ECM associate with the emergence of aggressive cancer cells with mesenchymal stem-like properties (35,36) and that TNC has itself been reported as a potential marker of CSCs (37-39), these bioinformatic findings led us to investigate and compare expression of CSC-associated genes (40) in responder and non-responder tumors. The data indicated that CSC genes are over-represented in non-responder compared to responder tumors (Fig. 6A,B). When tumors were stained for ZEB1, high ZEB1 expression was seen in control and non-responder compared to a dramatic decrease in responder tumors (Fig. 6C). This finding indicated that cancer cells in untreated and non-responder tumors were more stem-like; a finding which was in line with their more rapid *in vivo* growth compared to responder tumors.

We were consistently successful in generating tumor cell-lines from untreated and non-responder mice but not from responder mice, suggesting an intrinsic failure

of cells from the latter tumors to self-renew. However, to confirm that CSCs were more abundant in non-responder compared to responder tumors, it was necessary to examine the ability of cells isolated from both tumor types to self-renew. A tumor sphere formation assay was performed by seeding equal numbers of live disaggregated tumor cells from untreated, non-responders and responder tumors in serum-free, non-adherent conditions (41). With this assay it is possible to determine the presence of CSCs or progenitor cells, since these are the only cell types capable of surviving and proliferating under such conditions (41). Tumorspheres with a diameter >50 μm were counted following two passages. Data showed that tumorspheres readily formed from untreated and non-responder tumors but not in responders (Fig. 6D, E). These findings indicated that a successful antitumor T cell response associated with a loss of CSCs. Overall, the data presented in this study showed that a sufficiently robust T cell response induced multiple changes to the TME, which served to drive elimination of tumor cells while concurrently amplifying the immune response.

Discussion

In this study, using a mouse model of carcinogen-induced tumors, we detected a relationship between the ECM protein, TNC, and a poor overall response to immunotherapy.

Since there are several reports describing an effect of the ECM on immune cells behaviour (7,26,30,42) including a negative effect of TNC on T cell function and motility (7,43), we questioned whether TNC hampered the ability of T cells, stimulated following Treg depletion, to effectively access and kill tumor cells (28,43,44). Our findings disproved this hypothesis as TNC expression before Treg depletion did not predict response to treatment; indeed, depletion of Tregs resulted in successful elimination of both TNC-high and TNC-low tumor cell lines. We did however find that a robust T cell response associated with a loss of TNC and other ECM alterations. Our data do not rule out the involvement of other immune cells in driving changes to the ECM. It has been documented that tumor associated macrophages play a role in altering TNC expression during tumor progression. Deligne *et al*. indicate that $CD206^{+}$ M2-like macrophages are enriched in TNC-rich tumors and associate with poorer control of tumor growth (45). Whereas ECM

deposition in the TME can be influenced by macrophages (46), we had no evidence that this was the case in Treg-depleted, carcinogen-induced fibrosarcomas.

Along with ECM genes, we observed that some stem cell associated and EMT genes were downregulated in responder compared to untreated and non-responder tumors indicating that an effective immune response associated with a less aggressive cancer cell genotype. Whether the decrease in TNC and CSC gene expression was due to loss of CSCs as a result of immune destruction or whether a strong immune response drives loss of ECM, which then drives changes in cancer cell gene expression patterns is yet to be determined. The latter hypothesis was supported by the demonstration that ECM proteins contributed to tumor progression through increasing tumor tension leading to biomechanical signalling cues which drive expression of CSC/EMT genes (36). Additionally, previous studies show that cognate, non-lytic interactions between T cells and cancer cells can promote expression of stem-like genes by cancer cells (47). It is possible that in our model, non-responder tumors may have become more stem-like and aggressive by avoiding lysis by cognate T cells.

The tumor promoting effects of ECM-mediated corruption of tissue tension are also linked to poorly developed lymphatic vessels, which serve to further increase intra-tumoral tensile forces (30,35,36). We found a striking difference in the appearance of lymphatic vessels in responder *versus* non-responder tumors in terms of organisation, density and CCL21 expression. These findings supported a scenario whereby loss of ECM associated with improved lymphatic function. This may both relieve intra-tumoral interstitial pressure and improve T cell response, through guiding migration of antigen-presenting $CCR7^{+}$ DCs to draining lymph nodes for priming T cells (34,48) further facilitating a switch from a predominantly immunosuppressive environment to a predominantly immunostimulatory one.

A picture is emerging which describes the ability of the immune system to initiate and direct remodelling of the TME in a manner which serves to amplify its antitumor activities. The mechanisms behind this split remain unknown. Methylcholanthrene is highly mutagenic making it possible that individual tumors exhibit different frequencies of neoantigens which define their immunogenicity. In this scenario, responder tumors may have many neoantigens whilst non-responders present fewer neoantigens (49,50). This hypothesis is supported by work that indicates that the selective expansion of certain T cell receptors in defined tumor regions correlates with the number of non-synonymous mutations at the same sites

(51). Our findings indicated that if a sufficiently robust T cell response was induced by immunotherapy, the balance was tipped whereby the ECM was lost, aiding lymphatic vessel function, HEV development and a self-amplifying immune response. This was accompanied by a reversal in CSC-associated gene expression and an intrinsic loss of cancer cell aggression. We propose that the simultaneous occurrence of these events is essential for creating the "perfect storm" required for successful antitumor immunity. This could be enhanced by empowering adoptively transferred T cells with the ability to digest the ECM and/or to improve endothelial cell function, or by combining cancer immunotherapies with anti-fibrotic treatments or treatments designed to improve the tumor vasculature. By altering the TME in this way, it may be possible to tip the balance in favor of the "perfect storm" even when the T cell response is sub-optimal.

Acknowledgements

We are grateful to the staff at Cardiff University JBIOS for their continued support, and Genentech for provision of PI-3065.

References

1. Emens LA, Ascierto PA, Darcy PK, Demaria S, Eggermont AMM, Redmond WL*, et al.* Cancer immunotherapy: Opportunities and challenges in the rapidly evolving clinical landscape. Eur J Cancer **2017**;81:116-29 doi 10.1016/j.ejca.2017.01.035.
2. Lohmueller J, Finn OJ. Current modalities in cancer immunotherapy: Immunomodulatory antibodies, CARs and vaccines. Pharmacol Ther **2017**;178:31-47 doi 10.1016/j.pharmthera.2017.03.008.
3. Hindley JP, Jones E, Smart K, Bridgeman H, Lauder SN, Ondondo B*, et al.* T-cell trafficking facilitated by high endothelial venules is required for tumor control after regulatory T-cell depletion. Cancer Res **2012**;72(21):5473-82 doi 10.1158/0008-5472.CAN-12-1912.
4. Colbeck EJ, Jones E, Hindley JP, Smart K, Schulz R, Browne M*, et al.* Treg Depletion Licenses T Cell-Driven HEV Neogenesis and Promotes Tumor Destruction. Cancer Immunol Res **2017**;5(11):1005-15 doi 10.1158/2326-6066.CIR-17-0131.
5. Allen E, Jabouille A, Rivera LB, Lodewijckx I, Missiaen R, Steri V*, et al.* Combined antiangiogenic and anti-PD-L1 therapy stimulates tumor immunity through HEV formation. Sci Transl Med **2017**;9(385) doi 10.1126/scitranslmed.aak9679.
6. Kraman M, Bambrough PJ, Arnold JN, Roberts EW, Magiera L, Jones JO*, et al.* Suppression of antitumor immunity by stromal cells expressing fibroblast activation protein-alpha. Science **2010**;330(6005):827-30 doi 10.1126/science.1195300.
7. Salmon H, Franciszkiewicz K, Damotte D, Dieu-Nosjean MC, Validire P, Trautmann A*, et al.* Matrix architecture defines the preferential localization

and migration of T cells into the stroma of human lung tumors. J Clin Invest **2012**;122(3):899-910 doi 10.1172/JCI45817.

8. Peske JD, Woods AB, Engelhard VH. Control of CD8 T-Cell Infiltration into Tumors by Vasculature and Microenvironment. Adv Cancer Res **2015**;128:263-307 doi 10.1016/bs.acr.2015.05.001.
9. Sautès-Fridman C, Petitprez F, Calderaro J, Fridman WH. Tertiary lymphoid structures in the era of cancer immunotherapy. Nat Rev Cancer **2019**;19(6):307-25 doi 10.1038/s41568-019-0144-6.
10. He B, Jabouille A, Steri V, Johansson-Percival A, Michael IP, Kotamraju VR, *et al.* Vascular targeting of LIGHT normalizes blood vessels in primary brain cancer and induces intratumoural high endothelial venules. J Pathol **2018**;245(2):209-21 doi 10.1002/path.5080.
11. Kim JM, Rasmussen JP, Rudensky AY. Regulatory T cells prevent catastrophic autoimmunity throughout the lifespan of mice. Nat Immunol **2007**;8(2):191-7 doi 10.1038/ni1428.
12. Hindley JP, Ferreira C, Jones E, Lauder SN, Ladell K, Wynn KK, *et al.* Analysis of the T-cell receptor repertoires of tumor-infiltrating conventional and regulatory T cells reveals no evidence for conversion in carcinogen-induced tumors. Cancer Res **2011**;71(3):736-46 doi 10.1158/0008-5472.CAN-10-1797.
13. Bankhead P, Loughrey MB, Fernández JA, Dombrowski Y, McArt DG, Dunne PD, *et al.* QuPath: Open source software for digital pathology image analysis. Scientific Reports **2017**;7(1):16878 doi 10.1038/s41598-017-17204-5.
14. Soady KJ, Tornillo G, Kendrick H, Meniel V, Olijnyk-Dallis D, Morris JS, *et al.* The receptor protein tyrosine phosphatase PTPRB negatively regulates FGF2-dependent branching morphogenesis. Development **2017**;144(20):3777-88 doi 10.1242/dev.149120.
15. Ritchie ME, Phipson B, Wu D, Hu Y, Law CW, Shi W, *et al.* limma powers differential expression analyses for RNA-sequencing and microarray studies. Nucleic Acids Res **2015**;43(7):e47 doi 10.1093/nar/gkv007.
16. Yu G, He QY. ReactomePA: an R/Bioconductor package for reactome pathway analysis and visualization. Mol Biosyst **2016**;12(2):477-9 doi 10.1039/c5mb00663e.
17. Durinck S, Moreau Y, Kasprzyk A, Davis S, De Moor B, Brazma A, *et al.* BioMart and Bioconductor: a powerful link between biological databases and microarray data analysis. Bioinformatics **2005**;21(16):3439-40 doi 10.1093/bioinformatics/bti525.
18. Newman AM, Liu CL, Green MR, Gentles AJ, Feng W, Xu Y, *et al.* Robust enumeration of cell subsets from tissue expression profiles. Nature Methods **2015**;12(5):453-7 doi 10.1038/nmeth.3337.
19. Sturm G, Finotello F, Petitprez F, Zhang JD, Baumbach J, Fridman WH, *et al.* Comprehensive evaluation of transcriptome-based cell-type quantification methods for immuno-oncology. Bioinformatics **2019**;35(14):i436-i45 doi 10.1093/bioinformatics/btz363.
20. Love MI, Huber W, Anders S. Moderated estimation of fold change and dispersion for RNA-seq data with DESeq2. Genome Biol **2014**;15(12):550 doi 10.1186/s13059-014-0550-8.
21. Marisa L, Svrcek M, Collura A, Becht E, Cervera P, Wanherdrick K, *et al.* The Balance Between Cytotoxic T-cell Lymphocytes and Immune Checkpoint Expression in the Prognosis of Colon Tumors. J Natl Cancer Inst **2018**;110(1) doi 10.1093/jnci/djx136.
22. Wickham H, Averick M, Bryan J, Chang W, McGowan8 LDA, François R, *et al.* Welcome to the Tidyverse. Journal of Open Source Software **2019**;4(43) doi 10.21105/joss.01686.

23. Oskarsson T, Acharyya S, Zhang XH, Vanharanta S, Tavazoie SF, Morris PG*, et al.* Breast cancer cells produce tenascin C as a metastatic niche component to colonize the lungs. Nat Med **2011**;17(7):867-74 doi 10.1038/nm.2379.
24. Lowy CM, Oskarsson T. Tenascin C in metastasis: A view from the invasive front. Cell Adh Migr **2015**;9(1-2):112-24 doi 10.1080/19336918.2015.1008331.
25. Gocheva V, Naba A, Bhutkar A, Guardia T, Miller KM, Li CM*, et al.* Quantitative proteomics identify Tenascin-C as a promoter of lung cancer progression and contributor to a signature prognostic of patient survival. Proc Natl Acad Sci U S A **2017**;114(28):E5625-E34 doi 10.1073/pnas.1707054114.
26. Onion D, Isherwood M, Shridhar N, Xenophontos M, Craze ML, Day LJ*, et al.* Multicomponent analysis of the tumour microenvironment reveals low CD8 T cell number, low stromal caveolin-1 and high tenascin-C and their combination as significant prognostic markers in non-small cell lung cancer. Oncotarget **2018**;9(2):1760-71 doi 10.18632/oncotarget.18880.
27. Galon J, Costes A, Sanchez-Cabo F, Kirilovsky A, Mlecnik B, Lagorce-Pagès C*, et al.* Type, density, and location of immune cells within human colorectal tumors predict clinical outcome. Science **2006**;313(5795):1960-4 doi 10.1126/science.1129139.
28. Mirzaei R, Sarkar S, Dzikowski L, Rawji KS, Khan L, Faissner A*, et al.* Brain tumor-initiating cells export tenascin-C associated with exosomes to suppress T cell activity. Oncoimmunology **2018**;7(10):e1478647 doi 10.1080/2162402X.2018.1478647.
29. Wehrhan F, Rödel F, Grabenbauer GG, Amann K, Brückl W, Schultze-Mosgau S. Transforming growth factor beta 1 dependent regulation of Tenascin-C in radiation impaired wound healing. Radiother Oncol **2004**;72(3):297-303 doi 10.1016/j.radonc.2004.07.011.
30. Acerbi I, Cassereau L, Dean I, Shi Q, Au A, Park C*, et al.* Human breast cancer invasion and aggression correlates with ECM stiffening and immune cell infiltration. Integr Biol (Camb) **2015**;7(10):1120-34 doi 10.1039/c5ib00040h.
31. Seager RJ, Hajal C, Spill F, Kamm RD, Zaman MH. Dynamic interplay between tumour, stroma and immune system can drive or prevent tumour progression. Convergent Science Physical Oncology2017.
32. Zuliani-Alvarez L, Marzeda AM, Deligne C, Schwenzer A, McCann FE, Marsden BD*, et al.* Mapping tenascin-C interaction with toll-like receptor 4 reveals a new subset of endogenous inflammatory triggers. Nat Commun **2017**;8(1):1595 doi 10.1038/s41467-017-01718-7.
33. Walker C, Mojares E, Del Río Hernández A. Role of Extracellular Matrix in Development and Cancer Progression. Int J Mol Sci **2018**;19(10) doi 10.3390/ijms19103028.
34. Vaahtomeri K, Brown M, Hauschild R, De Vries I, Leithner AF, Mehling M*, et al.* Locally Triggered Release of the Chemokine CCL21 Promotes Dendritic Cell Transmigration across Lymphatic Endothelia. Cell Rep **2017**;19(5):902-9 doi 10.1016/j.celrep.2017.04.027.
35. Northey JJ, Przybyla L, Weaver VM. Tissue Force Programs Cell Fate and Tumor Aggression. Cancer Discov **2017**;7(11):1224-37 doi 10.1158/2159-8290.CD-16-0733.
36. Laklai H, Miroshnikova YA, Pickup MW, Collisson EA, Kim GE, Barrett AS*, et al.* Genotype tunes pancreatic ductal adenocarcinoma tissue tension to induce matricellular fibrosis and tumor progression. Nat Med **2016**;22(5):497-505 doi 10.1038/nm.4082.

37. Nie S, Gurrea M, Zhu J, Thakolwiboon S, Heth JA, Muraszko KM*, et al.* Tenascin-C: a novel candidate marker for cancer stem cells in glioblastoma identified by tissue microarrays. J Proteome Res **2015**;14(2):814-22 doi 10.1021/pr5008653.
38. He J, Liu Y, Xie X, Zhu T, Soules M, DiMeco F*, et al.* Identification of cell surface glycoprotein markers for glioblastoma-derived stem-like cells using a lectin microarray and LC-MS/MS approach. J Proteome Res **2010**;9(5):2565-72 doi 10.1021/pr100012p.
39. Pezzolo A, Parodi F, Marimpietri D, Raffaghello L, Cocco C, Pistorio A*, et al.* Oct-4+/Tenascin C+ neuroblastoma cells serve as progenitors of tumor-derived endothelial cells. Cell Res **2011**;21(10):1470-86 doi 10.1038/cr.2011.38.
40. Zhang P, Sun Y, Ma L. ZEB1: at the crossroads of epithelial-mesenchymal transition, metastasis and therapy resistance. Cell Cycle **2015**;14(4):481-7 doi 10.1080/15384101.2015.1006048.
41. Johnson S, Chen H, Lo PK. Tumorsphere Formation Assays. Bio Protoc **2013**;3(3).
42. Salmon H, Donnadieu E. Within tumors, interactions between T cells and tumor cells are impeded by the extracellular matrix. Oncoimmunology **2012**;1(6):992-4 doi 10.4161/onci.20239.
43. Parekh K, Ramachandran S, Cooper J, Bigner D, Patterson A, Mohanakumar T. Tenascin-C, over expressed in lung cancer down regulates effector functions of tumor infiltrating lymphocytes. Lung Cancer **2005**;47(1):17-29 doi 10.1016/j.lungcan.2004.05.016.
44. Puente Navazo MD, Valmori D, Rüegg C. The alternatively spliced domain TnFnIII A1A2 of the extracellular matrix protein tenascin-C suppresses activation-induced T lymphocyte proliferation and cytokine production. J Immunol **2001**;167(11):6431-40.
45. Deligne C, Murdamoothoo D, Gammage AN, Gschwandtner M, Erne W, Loustau T*, et al.* Matrix-Targeting Immunotherapy Controls Tumor Growth and Spread by Switching Macrophage Phenotype. Cancer Immunology Research **2020**;8(3):368-82 doi 10.1158/2326-6066.Cir-19-0276.
46. Liguori M, Solinas G, Germano G, Mantovani A, Allavena P. Tumor-Associated Macrophages as Incessant Builders and Destroyers of the Cancer Stroma. Cancers **2011**;3(4):3740-61.
47. Stein RG, Ebert S, Schlahsa L, Scholz CJ, Braun M, Hauck P*, et al.* Cognate Nonlytic Interactions between CD8+ T Cells and Breast Cancer Cells Induce Cancer Stem Cell–like Properties. Cancer Research **2019**;79(7):1507-19 doi 10.1158/0008-5472.Can-18-0387.
48. Russo E, Teijeira A, Vaahtomeri K, Willrodt AH, Bloch JS, Nitschké M*, et al.* Intralymphatic CCL21 Promotes Tissue Egress of Dendritic Cells through Afferent Lymphatic Vessels. Cell Rep **2016**;14(7):1723-34 doi 10.1016/j.celrep.2016.01.048.
49. Schumacher TN, Schreiber RD. Neoantigens in cancer immunotherapy. Science **2015**;348(6230):69-74 doi 10.1126/science.aaa4971.
50. Alspach E, Lussier DM, Miceli AP, Kizhvatov I, DuPage M, Luoma AM*, et al.* MHC-II neoantigens shape tumour immunity and response to immunotherapy. Nature **2019**;574(7780):696-701 doi 10.1038/s41586-019-1671-8.
51. Joshi K, Robert de Massy M, Ismail M, Reading JL, Uddin I, Woolston A*, et al.* Spatial heterogeneity of the T cell receptor repertoire reflects the mutational landscape in lung cancer. Nature Medicine **2019**;25(10):1549-59 doi 10.1038/s41591-019-0592-2.

Figure Legends

Figure 1. Gene and Protein expression of TNC in non-responding tumors to Treg depletion.

A, Schematic representation of T cell numbers and HEVs between untreated, non-responder and responder tumors, as described in Ref 3 and 4. **B**, Differential expression analysis of microarray data comparing the three groups using the R package limma. Venn diagrams show the number of significantly differentially expressed genes (padj < 0.05) for each group comparison (gene significant in both are at the intersect of the comparison circles). Heatmaps showing differentially expressed genes which are upregulated **C**, or downregulated **D**, in non-responder relative to responder tumors. **E**, Representative high-power images of at least 10 samples per group with corresponding low power image of $CD3^+$ cells (red) in tumors, with validation of TNC expression (green) in each group. Scale bars are indicated in each image. **F,** Representative high-power images of 5 samples per group with corresponding low power image of whole tumor sections stained for TNC mRNA transcripts (pink) expression. Scale bars are indicated in each image. **G,** Representative high-power image of 15 samples of TNC mRNA transcripts (red) located on the cytoplasm of cells. Scale bar, 10 μm.

Figure 2. Low TNC expression correlated with patient survival only in tumors with high expression of a cytotoxic gene signature.

A, Kaplan Meier (KM) survival analysis of 14 cancers in which a CTL gene signature was associated with longer survival (based on survival curves shown in Supplemental Fig. S4A), patients have been clustered by CTL gene expression in their primary tumor. CTL High tumors (N=1590, orange line) were used to cluster patients by TNC expression (**B**). Blue line, TNC Low primary tumors (N=1187) and red line, TNC high (N=403). CTL Low tumors (N=4338, green line in A) were used to cluster patients by TNC expression (**C**)**.** TNC Low primary tumors (N=3361, blue line) and TNC high (N=977, red line). Individual plots for each cancer are shown in Supplemental Fig. S4. Significance was defined by a log rank p-value (P < 0.05).

Figure 3. TNC in the TME was not a barrier to T cell infiltration but impacts CTL degranulation.

A, High power images of TNC high (green, upper panel) and TNC low (bottom panel) areas with T cell infiltrates (red). Scale bars, 50 μm. **B**, Number of intratumoral $CD3^+$ cells in TNC high and low areas in untreated (*N*=8) and non-responder (*N*=5) tumors. Data are presented as individual data points (individual mice) plus median and standard error of the mean. Statistical significance was determined with Mann-Whitney test (**, P < 0.01). **C**, High power representative image of a $CD8^+GZMB^-$ cell (yellow arrowhead), $CD8^+GZMB^+$ cell (orange arrowhead) and $CD8^-GZMB^+$ cell (red arrowhead). CD8, blue; GZMB, red; TNC, green. Scale bars, 20 μm. **D**, Number of $CD8^+$ $GZMB^-$ and $CD8^+$ $GZMB^+$ cells in TNC high and low areas, in untreated (*N*=4) and non-responder tumors (*N*=10). Data are presented as individual data points (individual mice) plus median and standard error of the mean. Statistical significance was determined by Mann-Whitney test (**, P < 0.01).

Figure 4. **Presence of TNC in the TME did not impair an immune response to Treg Depletion**

A, Relative gene expression of TNC in Non-Infected (NI) cells, cells transfected with shScr, with shTNC 2475 and shTNC 3559 plasmids. Data are presented as median and standard error of the mean. Experiment was performed in triplicate. Statistical significance was determined by Kruskal-Wallis test with Dunn's multiple comparison test (*, P < 0.05). **B**, Tumor growth curves of shScr and shTNC tumors, untreated and Treg depleted. Data are presented as individual curves (individual mice, left) or as median and standard error of the mean (centre and right). *N*=4 shScr Untreated, Treg depleted and shTNC Treg depleted groups; *N*=3 shTNC untreated group. Statistical significance was determined by Kruskal-Wallis test with Dunn's multiple comparison test (*, P < 0.05; **, P < 0.01). **C**, Representative high-power images of at least 3 samples per group with corresponding low power image of TNC (green) expression and $CD3^+$ cell (red) infiltration. Scale bars are indicated in each image. **D**, Representative high-power images of 5 samples per group with corresponding low power image of $CD8^+$ cells (red) infiltration in untreated, and PI3065 treated 4T1 tumors, with TNC expression (green) in each group. Scale bars are indicated in each image.

Figure 5. Contrasting Expression of ECM Genes and Proteins between responders and Non-Responders.

A, Heatmap showing median normalised expression of genes belonging to the ECM organisation pathway in responders (R) and non-responders (NR). Only genes with an absolute mean difference greater than 0.5 between the two groups are shown. Arrows indicate genes Lumican (Lum) and Collagen type III a (Col3a1). **B-D**, Representative high-power images of at least 10 samples per group with corresponding low power image of whole tumors stained for Lumican (**B**, red), Collagen type III a (**C**, green), and LYVE-1 (green) and CCL21 (**D**, red) expression. Scale bars are indicated in each image.

Figure 6. Non-Responder Tumors Exhibited Enhanced Properties of CSCs.

A, Gene expression of genes associated with CSCs in responding and non-responding tumors. **B,** Comparison of median normalised gene expression of CSC genes in responder (blue) and non-responder (red) tumors. Individual values are shown as points while the mean expression is plotted by the connecting line. **C**, Representative high-power images of 5 samples per group with corresponding low power image of whole tumor stained Zeb-1 (green) expression. Scale bars are indicated in each image. **D**, Tumorsphere formation in cultures from untreated, non-responder, and responder tumors. **E**, Number of spheres formed after 14 days of culture, per 10^4 cells seeded. Data are presented as individual data points (individual mice) plus median and standard error of the mean. Statistical significance was determined with Kruskal-Wallis test ($P < 0.05$).

Figure 1

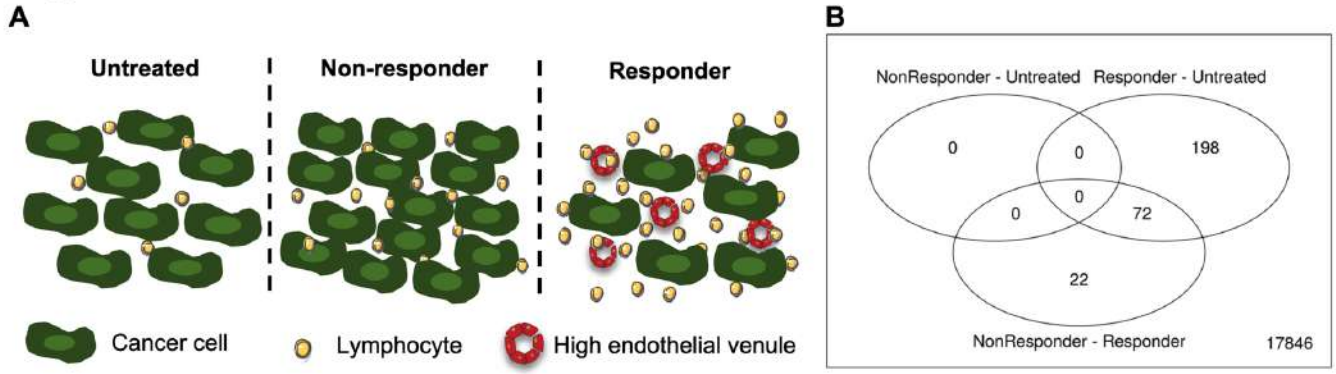

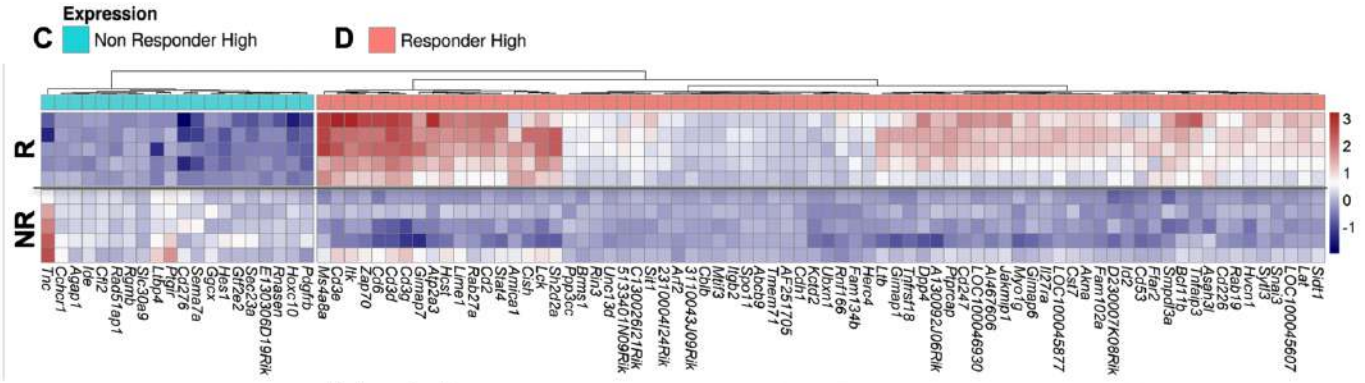

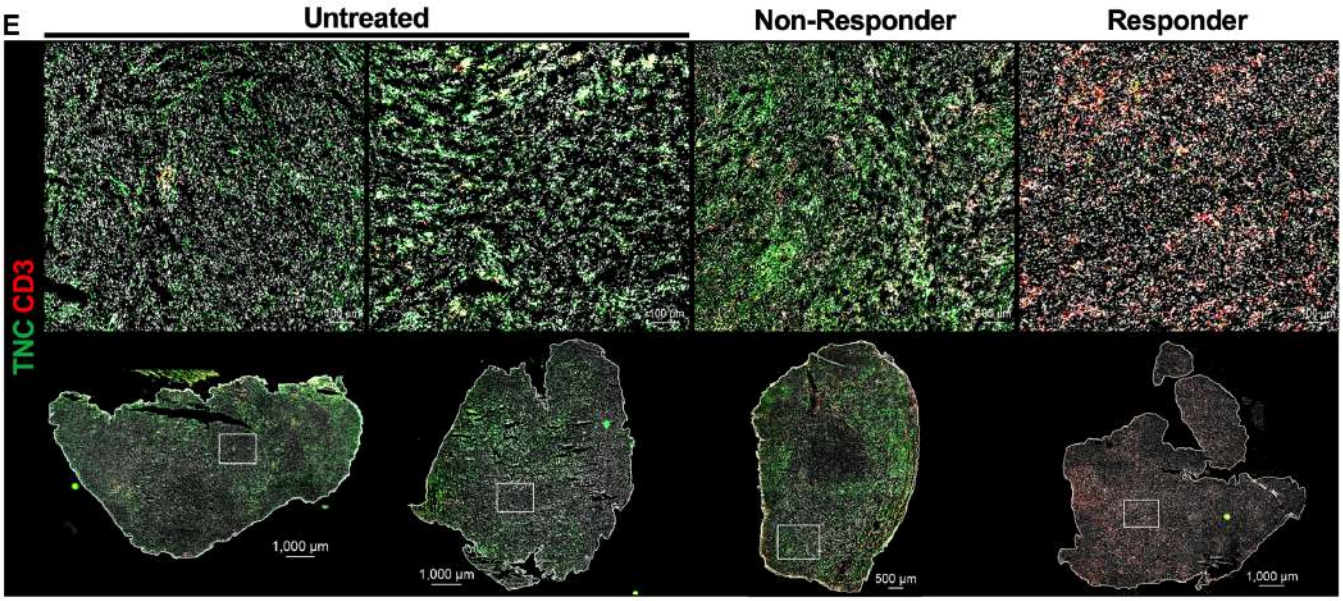

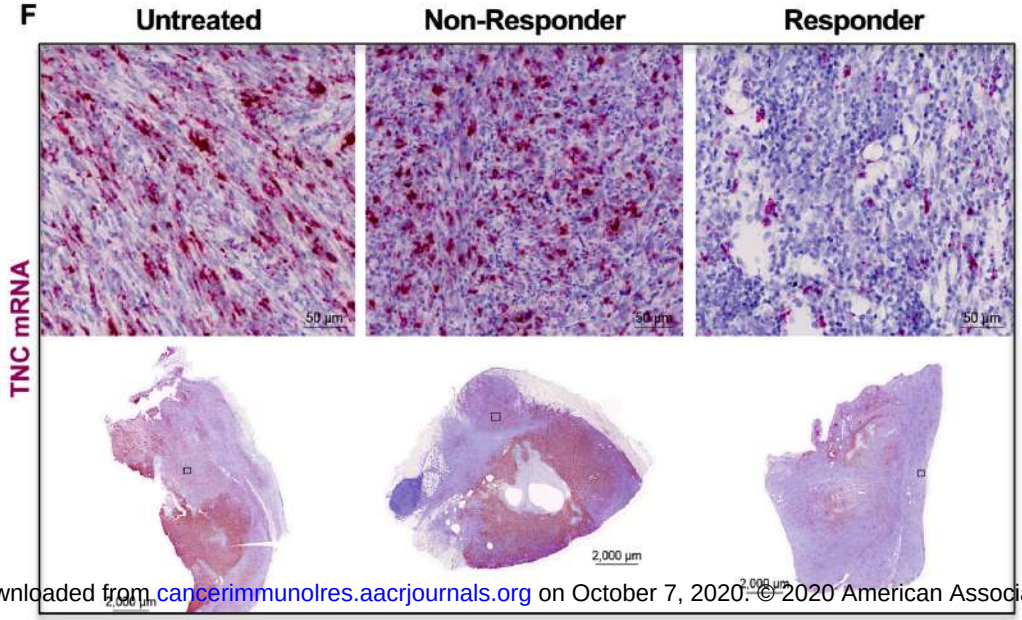

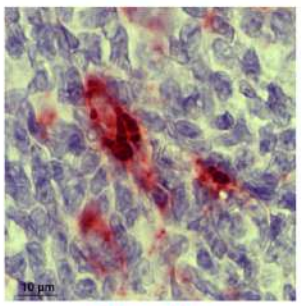

Figure 2

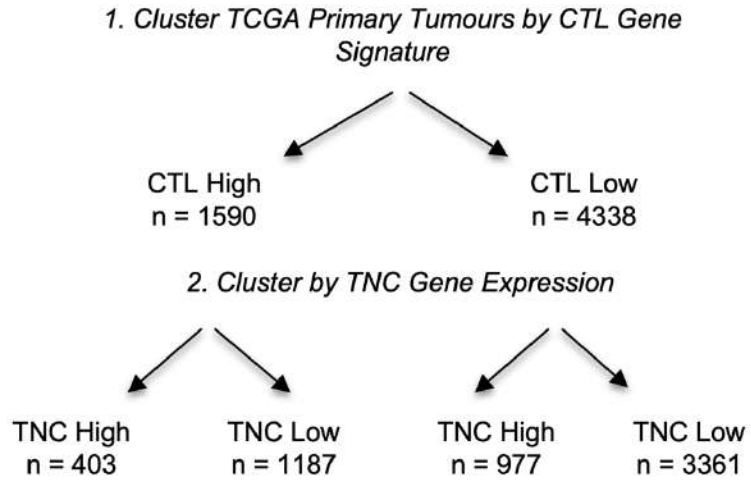

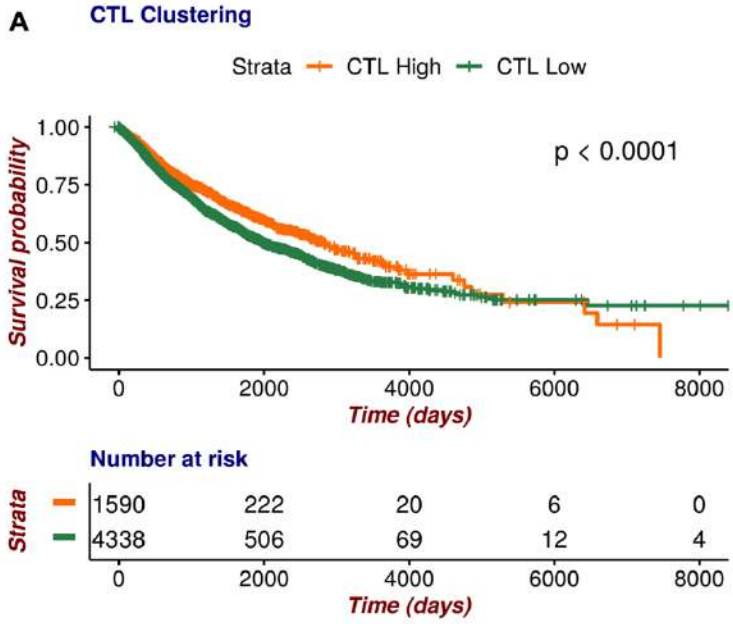

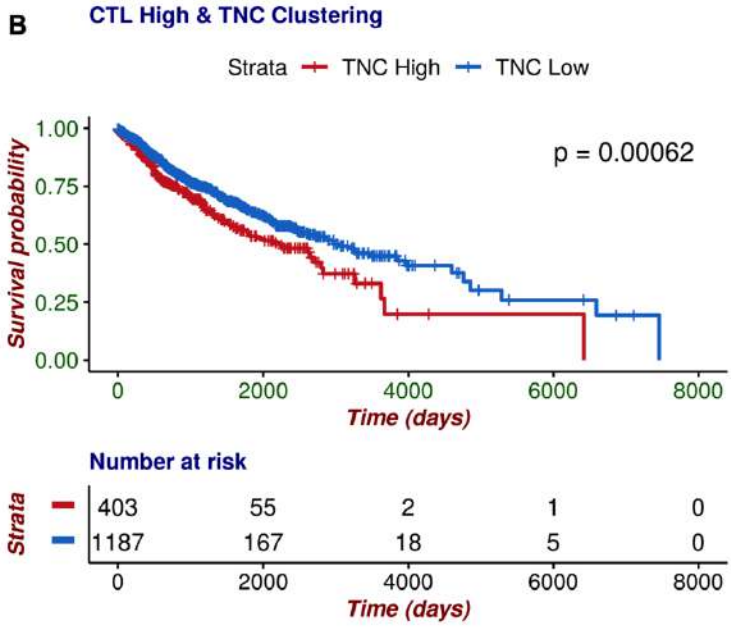

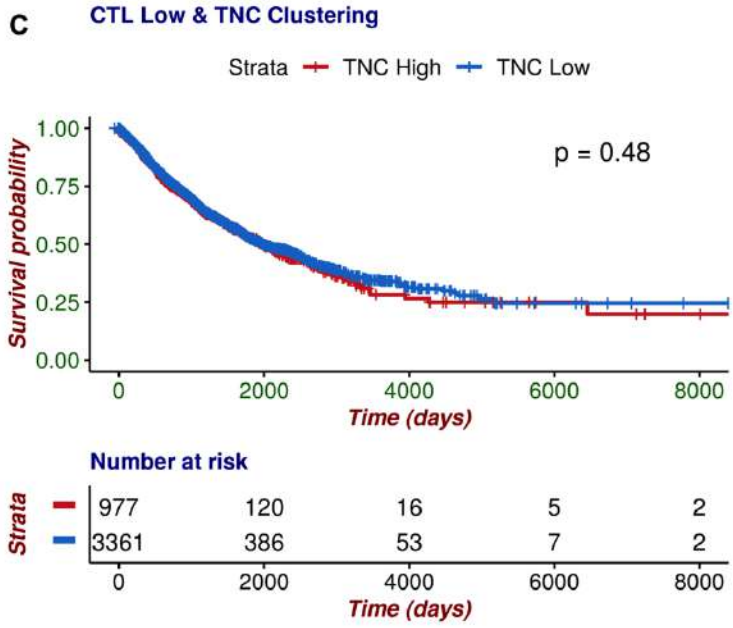

Figure 3

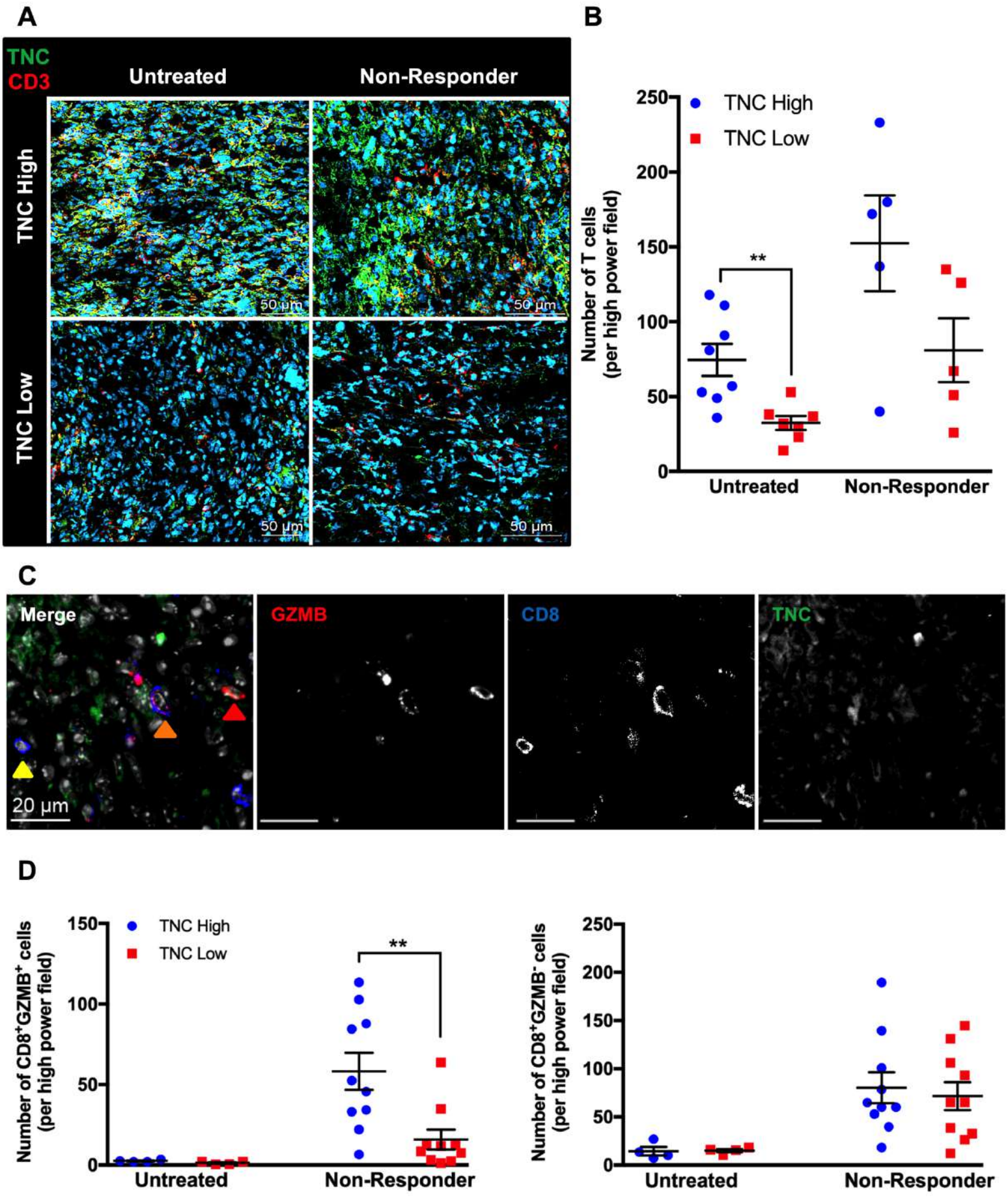

Figure 4

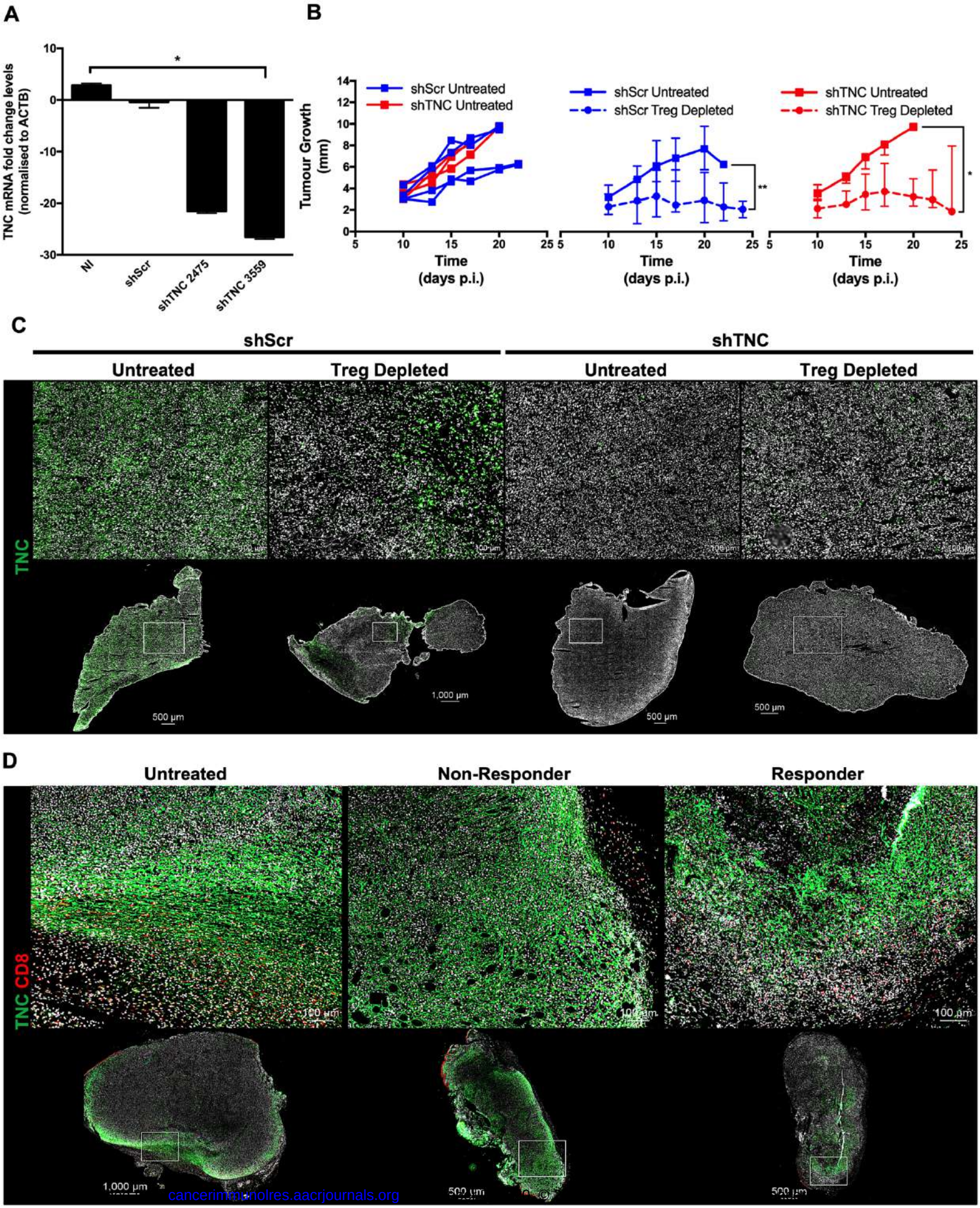

Figure 5

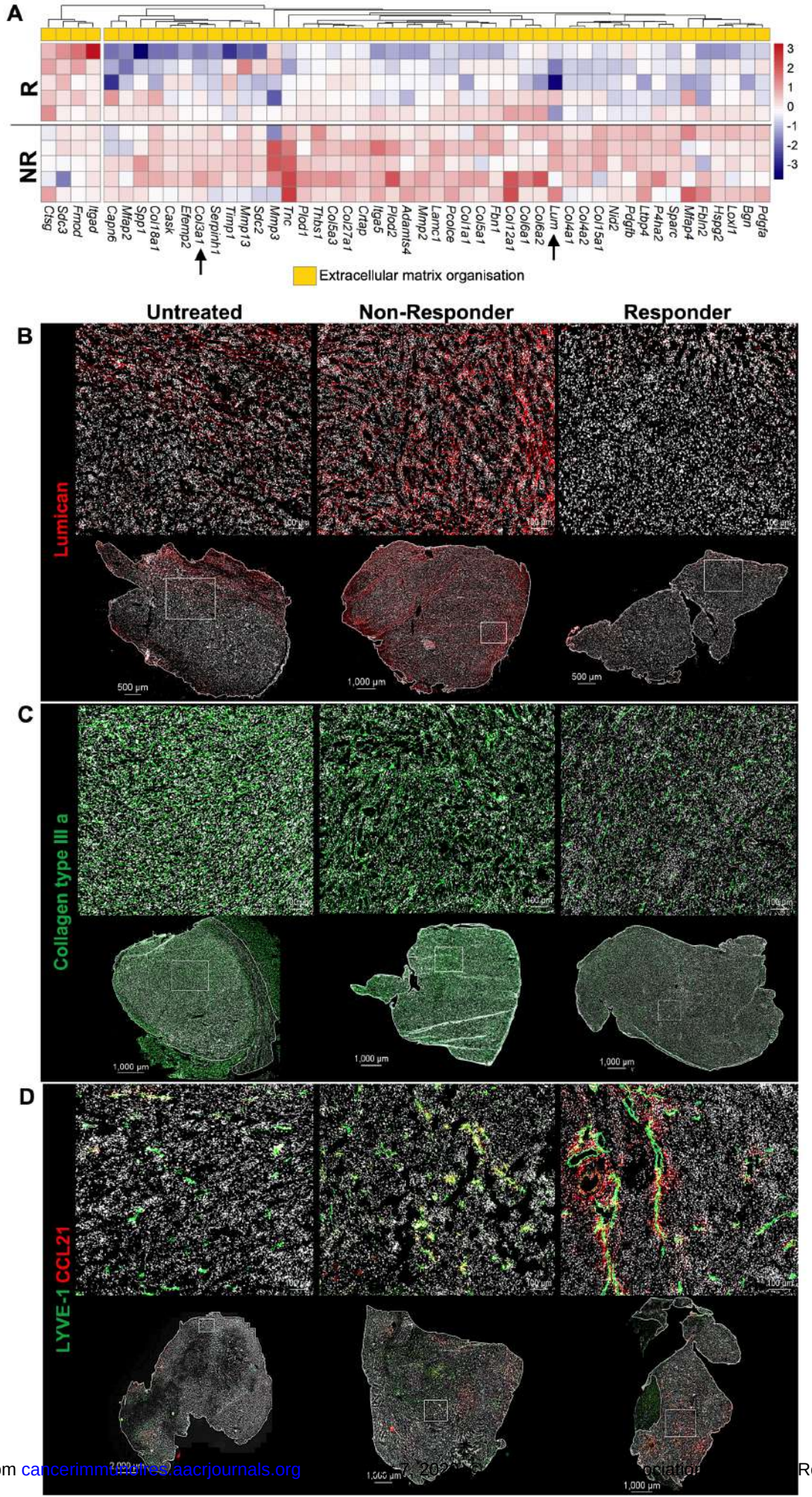

Figure 6

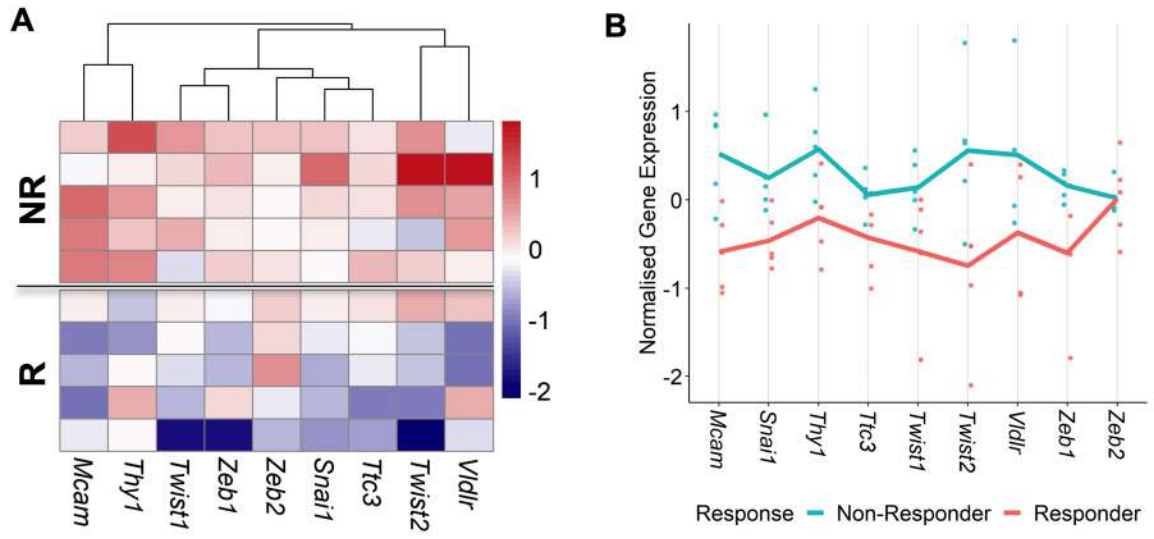

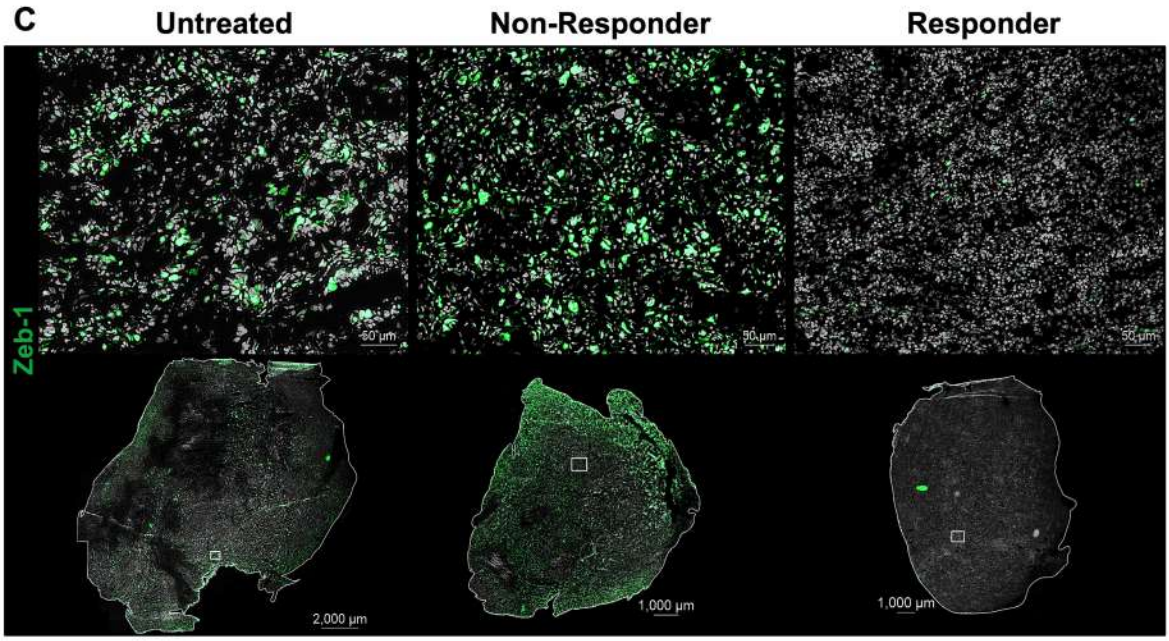

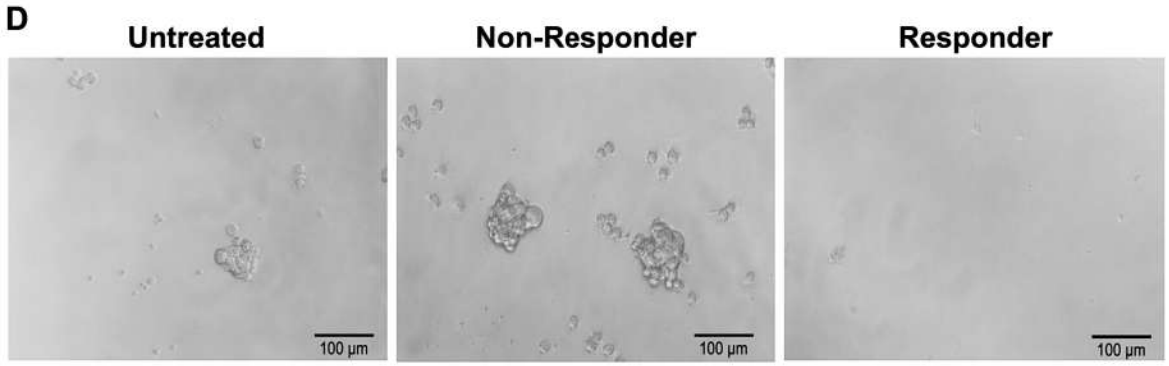

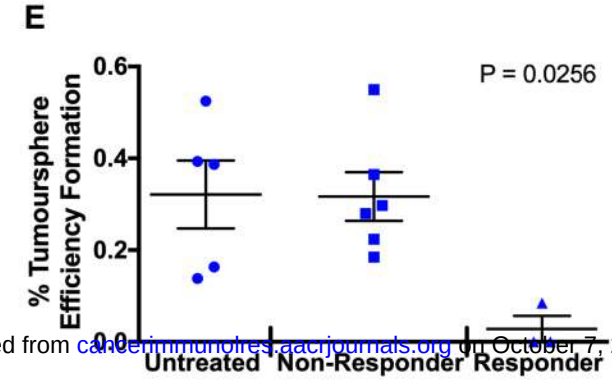

AACR American Association for Cancer Research

Cancer Immunology Research

Immune Remodelling of the Extracellular Matrix Drives Loss of Cancer Stem Cells and Tumor Rejection

Ana Pires, Alexander Greenshields-Watson, Emma Jones, et al.

Cancer Immunol Res Published OnlineFirst October 6, 2020.